Supplement of Earth Syst. Sci. Data, 18, 3587–3607, 2026
https://doi.org/10.5194/essd-18-3587-2026-supplement

Open Access Earth System Science Data

Supplement of

A Reanalysis-Based Global Tropical Cyclone Tracks Dataset for the Twentieth Century (RGTracks-20C)

Guiling Ye et al.

Correspondence to: Jeremy Cheuk-Hin Leung (chleung@pku.edu.cn) and Wenjie Dong (dongwj3@mail.sysu.edu.cn)

Introduction

This supporting information provides supplementary texts, figures, and tables cited in the main text.

S1 Tracker Detection Performance

Detailed figures comparing the Tracker's performance and characterizing the attributes of TC hits, misses, and false alarms are provided in this section.

S1.1 Validity of trackers

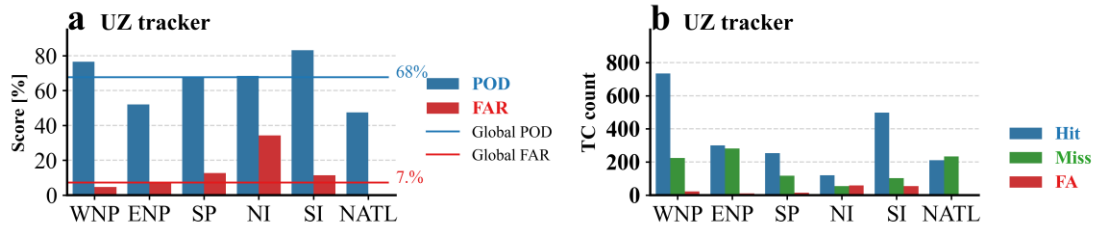

Figure S1: As in Fig. 3, but for the UZ tracker.

Table S1: The probability of detection (POD) and false alarm rate (FAR) of the global TCs detected by different trackers in the fifth generation ECMWF reanalysis (ERA5) and 20CRv3. POD (unit: %) and FAR (unit: %) of TCs detected by different trackers in the latest high-resolution ERA5 reanalysis by (Accarino et al., 2023) (green background), (Bourdin et al., 2022) (green background), UZ tracker (gray background) and RGTracks-20C (orange background).

	Hybrid[1]	CNRM[2]	TRACK[2]	UZ-ERA5[2]	OWZ-ERA5[2]	UZ-20CRv3	OWZ-20CRv3
POD (%)	71.49	72.77	74.37	71.54	71.75	67.62	76.56
FAR (%)	23	8.62	17.19	3.37	17.43	7.19	15.21

S1.2 Characteristics of hit, missed, and false-alarm TCs

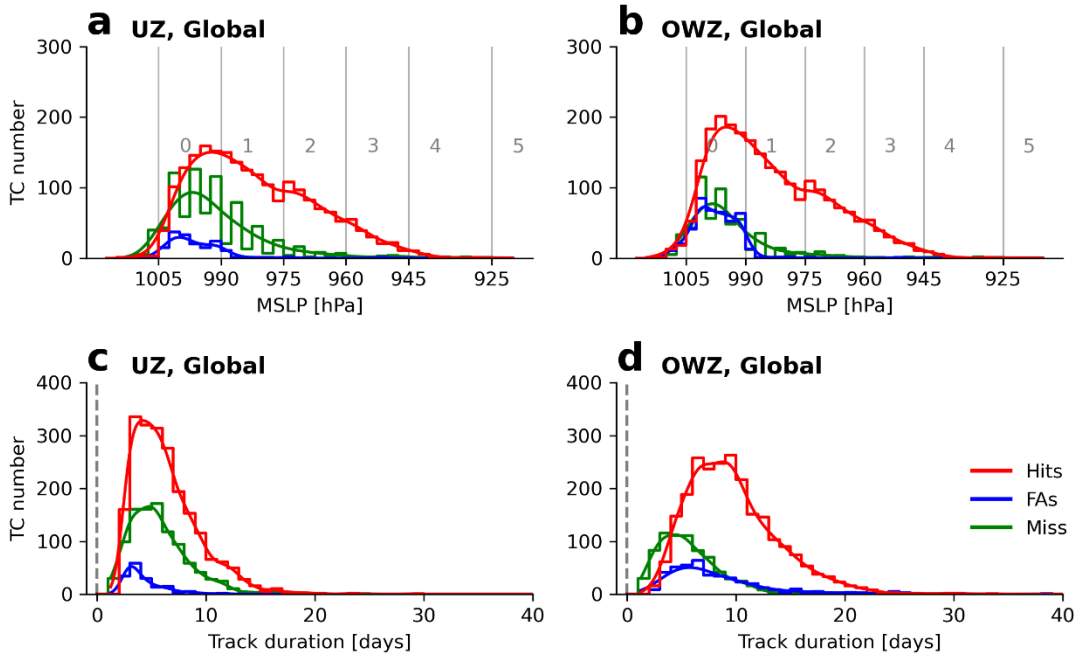

Figure S2: Properties of Hits, Misses, and False Alarms tracks for TC Trackers. a–b, Histograms of Hits (red), Misses (green), and FAs (blue) TC cases against TC intensity (minimum sea level pressure (SLP_{min}), unit: *hPa*, with the storm categories as defined according to '*TC classification' shown with vertical gray lines) detected by the UZ (**a**) and OWZ (**b**) trackers. **c–d,** same as **a–b**, except for histograms of Hits (red), Misses (green), and FAs (blue) TC cases against TC duration (unit: days).

The differences between RGTracks-20C and IBTrACS are most evident in the ENP, NATL, and NI. In the ENP and NATL, missed detections account for a relatively large fraction of the discrepancies, and most of these missed systems are weak and short-lived (Figs. S3a–h). By contrast, the NI is characterized more by a higher fraction of false alarms, which are mainly category 0–1 systems and tend to have relatively longer lifetimes (Figs. S3i–l). In addition to tracker-related limitations, these differences may also reflect uncertainties in the observational record in this basin.

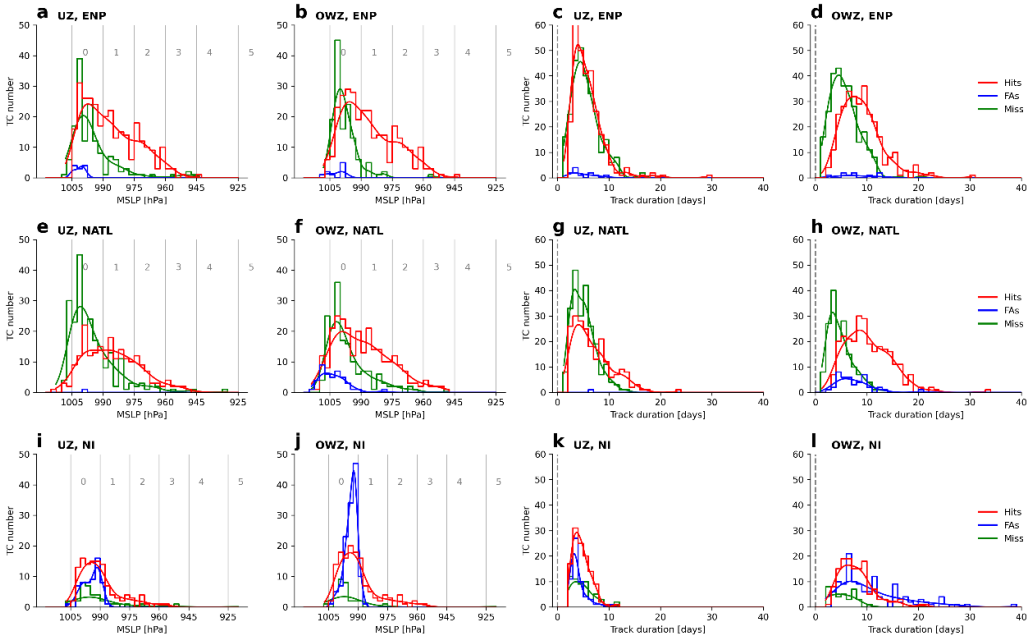

Figure S3: As in Fig. S2, but for the ENP, NATL, and NI. a–b, ENP, e–h, NATL, and i–l, NI. Histograms of TC intensity (SLP_{min}, unit: *hPa*) for the UZ tracker (a, e, i) and OWZ tracker (b, f, j), respectively. Histograms of TC duration (unit: days) for the UZ tracker (c, g, k) and OWZ tracker (d, h, l), respectively.

S2 Comparative Assessment of the UZ and OWZ Trackers

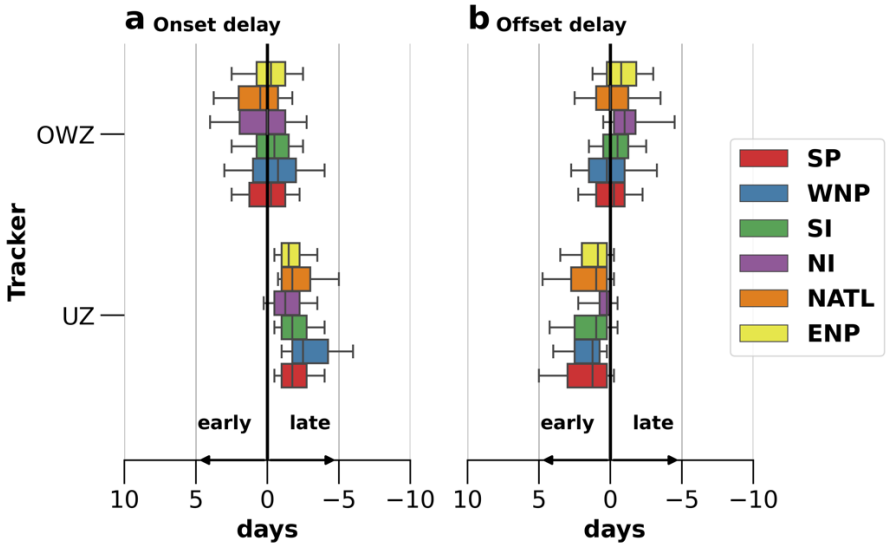

Figure S4: Onset and offset delays in TC detection by OWZ and UZ trackers. Onset delay (a): the delay between the first detection by both trackers and the first record in IBTrACS. Offset delay (b): the delay between the last detection by both trackers and the last record in IBTrACS. Colors represent different ocean basins: South Pacific (SP) (red), western North Pacific (WNP) (blue), South Indian (SI) (green), NI (purple), NATL (orange), and ENP (yellow). Box plots indicate the 25th, 50th, and 75th percentiles, whiskers show the 10th and 90th percentiles, and outliers are not shown.

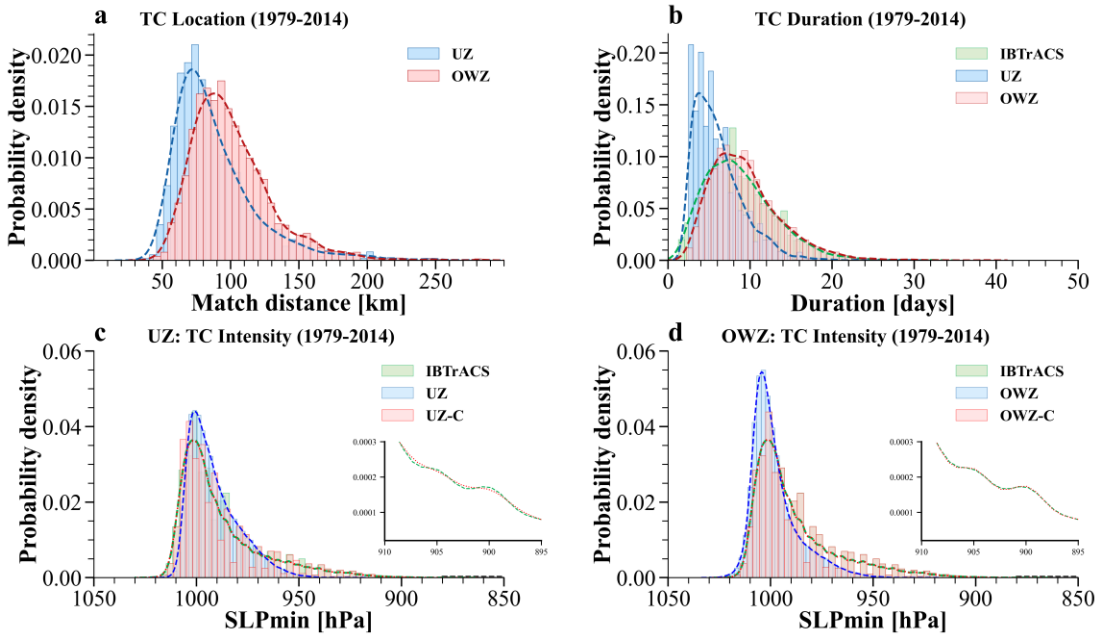

Figure S5: Distribution of TC characteristics om the IBTrACS and RGTracks-20C. a, Distribution of the mean TC location error from 1979–2014 (unit: km) between IBTrACS and the RGTracks-20C by the UZ (blue) and OWZ (red) algorithms. b, TC duration (unit: days) from 1979 to 2014 in IBTrACS (green) and the RGTracks-20C by the UZ (blue) and OWZ (red) algorithms. c, same as (b), but for TC intensity (*SLPmin*, unit: *hPa*), based on the UZ tracker, before (blue) and after (red) bias correction. d, same as (c), but for the OWZ tracker. (UZ: UZ tracker, OWZ: OWZ tracker. UZ-C and OWZ-C represent bias-corrected results for the UZ and OWZ trackers, respectively.)

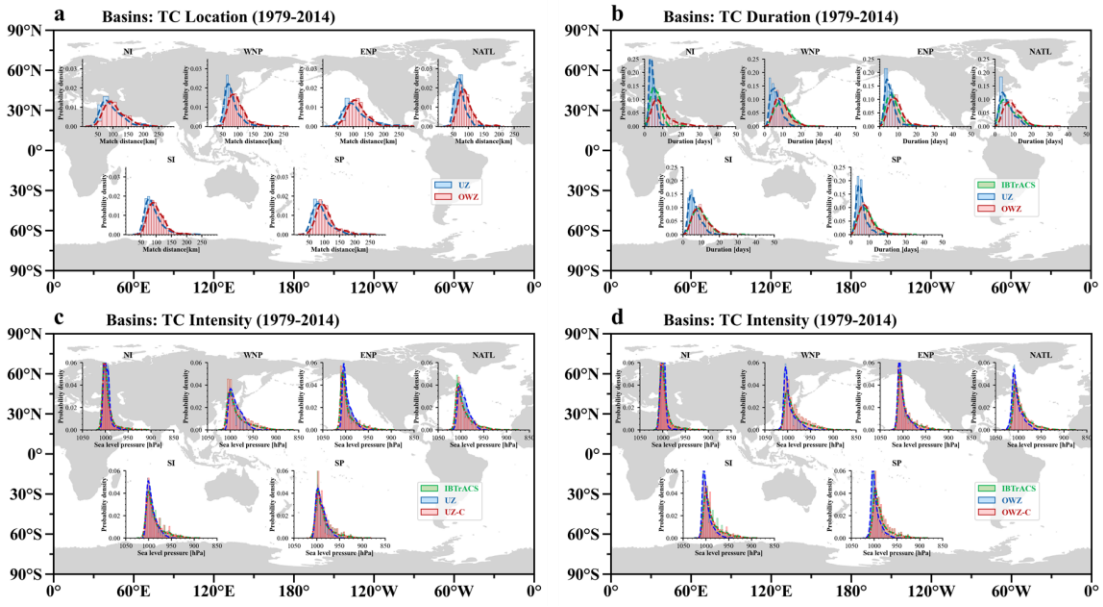

Figure S6: As in Fig. S4, but for six individual basins.

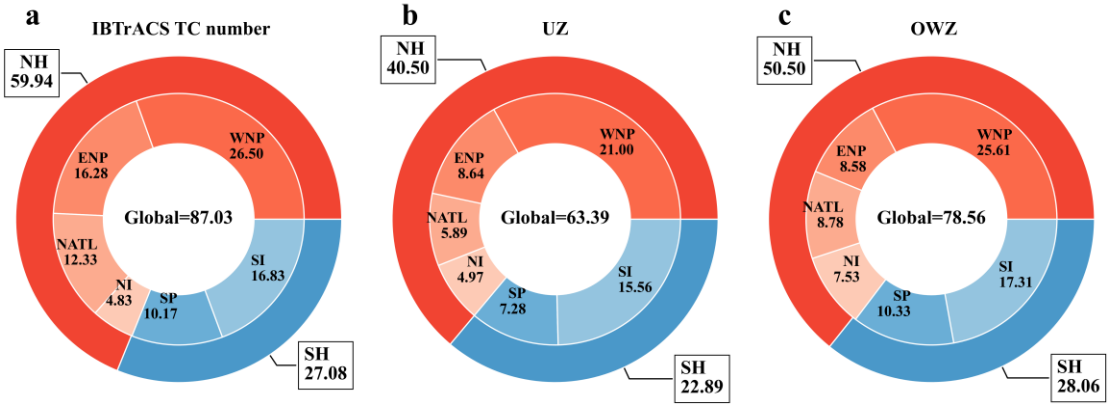

Figure S7: The mean number of TCs per year globally and for the six basins from IBTrACS (a), and using the UZ (b) and OWZ (c) trackers.

S3 ENP and NI

Table S2: Correlation coefficients of TC activity (number, days, intensity) in the ENP and NI between IBTrACS, RGTracks-20C and UZ tracker's results. This study initially verified the reliability of RGTracks-20C from 1979-2014. However, considering the lack of observational data, the study periods for ENP and NI were selected from 1988-2014 and 1990-2014, respectively. Asterisks indicate the confidence levels,1 asterisk (*) = 90%, 2 asterisks (**) = 95%, and 3 asterisks (***) = 99%.

Basin	Characteristics	Period	UZ	RGTracks-20C
ENP	Number	1979-2014	0.41**	0.35**
		1988-2014	0.77***	0.82***
	Duration	1979-2014	0.65***	0.58***
		1988-2014	0.89***	0.87***
	Intensity	1979-2014	0.01	0.15
		1988-2014	0.74***	0.66***
	Intensity-C	1979-2014	-0.02	0.11
		1988-2014	0.71***	0.67***
NI	Number	1979-2014	0.49***	0.54***
		1990-2014	0.58***	0.61***
	Duration	1979-2014	0.62***	0.34**
		1990-2014	0.63***	0.38*
	Intensity	1979-2014	0.48***	0.36**
		1990-2014	0.69***	0.62***
	Intensity-C	1979-2014	0.55***	0.47***
		1990-2014	0.68***	0.68***

Table S3: Starting years of TC intensity (SLP_{min}) recordings by different agencies across major ocean basins. (Information provided by Dr. Jennifer Gahtan, NOAA's National Center for Environmental Information.)

Basin	Agencies							
North Atlantic	HURDAT2	M Chenoweth	DS824	TD9636				
	1979*1	1851	1851	1899				
East Pacific	HURDAT2		DS824					
	1988	0	1949					
Central Pacific	HURDAT2							
	2001							
West Pacific	China	Japan	HKO	JTWC	DS824	TD9636		
	1949	1951	1961	2001	1945	1945		
North Indian Ocean	India	JTWC	DS824					
	1990*2	2001	Mid-19070's					
Southern Hemisphere	La Reunion	Australia	New Zealand,	Nadi	JTWC	DS824	Neumann	TD9636
	1977	1907	1968	1992	2001	1877	1960s	1956

Note:

*1. North Atlantic: 1979 (with prior data given if there was a specific observation) HURDAT2.

*2. North Indian Ocean: 1990 (soon to be 1982) India.

3. Multiple Basins 1945 TD9635.

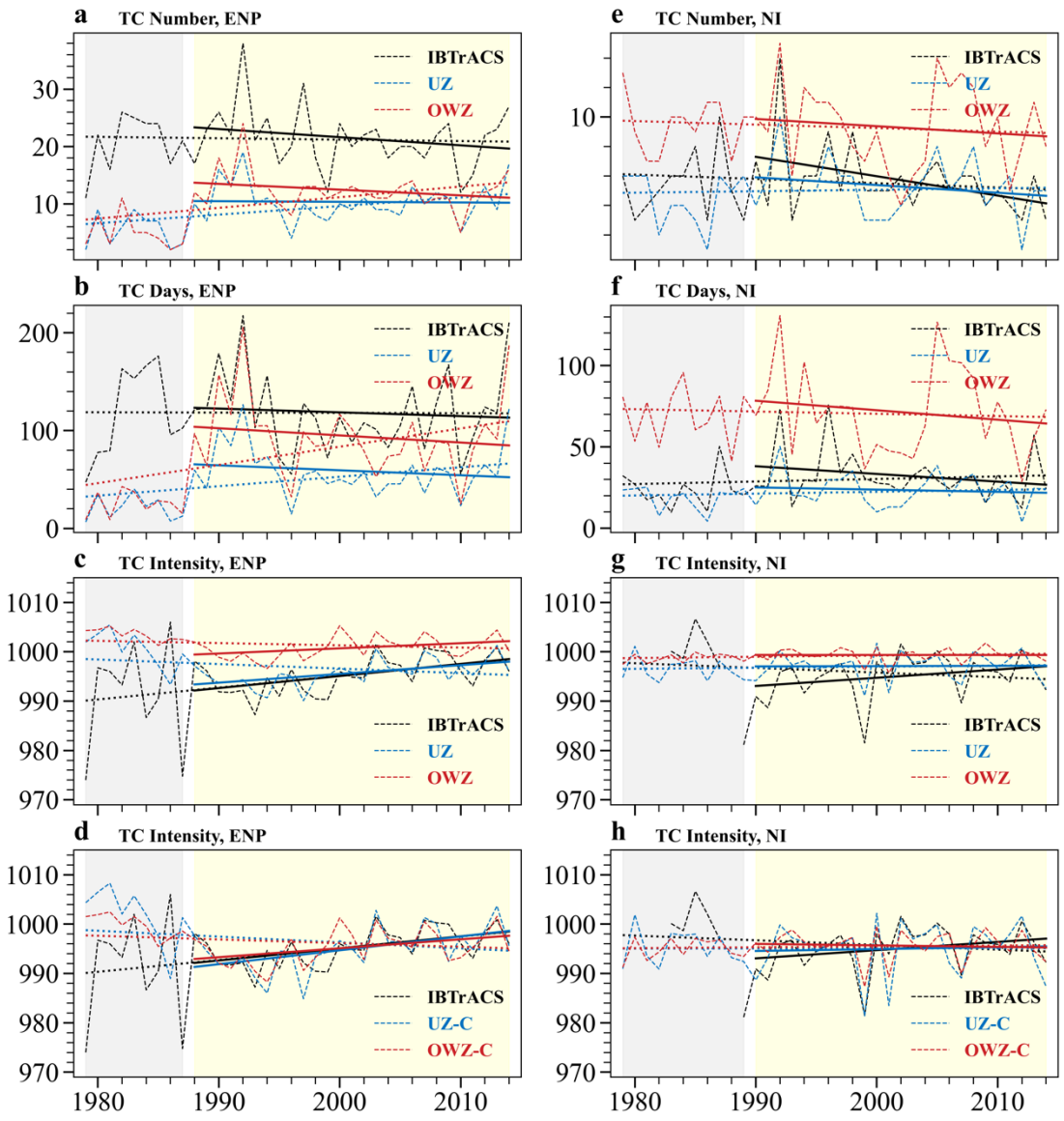

Figure S8: As in Fig. 4, but for the ENP and NI. a-d, time series and trends of TC number (unit: $year^{-1}$) (a), days (unit: $day \cdot year^{-1}$) (b), and intensity (unit: $hPa \cdot year^{-1}$) before correction (c) and after bias correction (d), as recorded by IBTrACS (black) and UZ tracker (blue), and RGTracks-20C (red) in the ENP. e-h, same as a-d, but for time series and trends of TC number (e), days (f), and intensity before correction (g) and after bias correction (h), as recorded by IBTrACS, RGTracks-20C and UZ tracker in the NI.

155 **S4 TC activity trends**

156 Although longer-term changes are not the primary focus of the present study, we briefly compare the
157 linear trends in TC activity between RGTracks-20C and IBTrACS in this section.
158 For TC number (Figs. 6a, 7a, and Table S4), based on IBTrACS, the WNP exhibit significant decreasing
159 trends of -0.12 $year^{-1}$. RGTracks-20C is able to reproduce the decreasing trends in these basins, with a
160 significant decrease of -0.12 $year^{-1}$ for the WNP. In the NATL basin, RGTracks-20C is able to reproduce
161 the significant increasing trend in TC number recorded by IBTrACS (0.24 $year^{-1}$), with the 0.14 $year^{-1}$
162 showing a significant increase consistent with observations. On a global scale, as well as in the NI and
163 SI, the trends observed by IBTrACS are not statistically significant, and RGTracks-20C yields consistent
164 results in these basins. Notably, in the ENP, there are significant differences in the long-term trends
165 between IBTrACS and RGTracks-20C
166 For TC days (Figs. 6b, 7b, and Table S4), the RGTracks-20C reproduces the significant decreasing trend
167 in the SP and the significant increasing trend in the NATL. In the WNP, the RGTracks-20C shows
168 agreement with the observed long-term trend, although the trends are not significant. In addition, at the
169 global scale and in the NI and SI, the RGTracks-20C well captures the observed insignificant long-term
170 trends of TC days. On the other hand, in the ENP, there is a significant difference in the slopes of the
171 long-term trends of IBTrACS and RGTracks-20C, which is consistent with the difference in the number
172 of TCs between them
173 For TC intensity, the IBTrACS shows a significant increase in TC intensity globally (0.17 $hPa \cdot year^{-1}$)
174 and in the SI (0.27 $hPa \cdot year^{-1}$), and the increasing trend is successfully reproduced by the RGTracks-
175 20C (Figs. 6c, 7c–d, and Table S4). In addition, the RGTracks-20C captures the insignificant trends in
176 TC intensity over the WNP, NATL, NI, and SP. In summary, the RGTracks-20C shows high consistency
177 with observations globally and in most regions. However, in the ENP, IBTrACS shows a significant
178 increasing trend, while RGTracks-20C shows a non-significant decreasing trend.
179 Overall, the RGTracks-20C can generally reproduce the trends of TC activity in IBTrACS globally and
180 over most of the basins. The corresponding UZ tracker's results also show similar longer-term behaviour
181 (Figs. 6a–c), but the agreement with IBTrACS is weaker than that of RGTracks-20C, especially in the
182 WNP, the most TC-active basin globally. Some discrepancies are observed in some specific basins,

especially the ENP and NI. These inconsistencies may be related to uncertainties in the observations and limitations of tracking algorithms. If the evaluation period is restricted to the 1980s, the correlation between RGTracks-20C and IBTrACS in recording TC activity improves significantly (Table S2), and more consistent long-term trend results are obtained (Table S5).

Table S4: Linear trends in TC activity globally and across six basins, as recorded in IBTrACS, RGTracks-20C and UZ tracker. Grey background indicates that the trends between IBTrACS and RGTracks-20C (UZ tracker) are consistent sign and statistical significance. Asterisks indicate the confidence levels,1 asterisk (*) = 90%, 2 asterisks (**) = 95%, and 3 asterisks (***) = 99%. UZ-C and OWZ-C represent results after intensity bias correction.

		Global	**WNP**	**ENP**	**NATL**	**NI**	**SI**	**SP**
Number ($year^{-1}$)	IBTrACS	**-0.06**	**-0.12***	-0.08	**0.24*****	**0.01**	**-0.04**	**-0.10***
	UZ	**-0.01**	**-0.14***	0.16***	**0.07**	**0.02**	**-0.01**	**-0.12****
	RGTracks-201	0.19	**-0.12***	0.20***	**0.14****	-0.04	0.04	**-0.08**
TC days ($day \cdot year^{-1}$)	IBTrACS	**-2.70**	**-3.64*****	-0.03	**1.93*****	**0.16**	**-0.15**	**-1.02***
	UZ	**-0.29**	**-0.95**	0.97**	**0.59**	**0.11**	**-0.40**	**-0.72***
	RGTracks-20C	1.82	**-1.32**	1.86***	**1.38****	-0.14	0.63	**-0.79***
Intensity ($hPa \cdot year^{-1}$)	IBTrACS	**0.17*****	**0.03**	0.24**	**-0.06**	-0.09	**0.27*****	**0.08**
	UZ	**0.03**	**0.01**	-0.09	**-0.06**	0.03	**0.05**	-0.06
	RGTracks-20C	**0.05*****	**0.03**	-0.05	**-0.05**	0.03	**0.08*****	**0.03**
	UZ-C	**0.04**	**0.02**	-0.12	**-0.10**	0.01	**0.07**	-0.10
	RGTracks-20C-C	**0.09*****	**0.04**	-0.07	**-0.08**	0.02	**0.13*****	**0.05**

Table S5: As in Table S4, but for ENP and NI. This study initially verified the reliability of RGTracks-20C and UZ-based results for the period 1979–2014. Due to limited observational data, the study periods for the ENP and NI basins were adjusted to 1988–2014 and 1990–2014, respectively.

Basin	Characteristics	Period	IBTrACS	UZ	RGTracks-20C
ENP	Number	1979-2014	-0.08	0.16*	0.20*
		1988-2014	**-0.04**	**0**	**-0.07**
	Duration	1979-2014	-0.03	0.97*	1.86*
		1988-2014	**-0.39**	**-0.51**	**-0.73**
	Intensity	1979-2014	0.24**	-0.09	-0.05
		1988-2014	**0.24*** **	**0.18*** **	**0.10***
	Intensity-C	1979-2014	0.24**	-0.12	-0.07
		1988-2014	**0.24***	**0.28*** **	**0.18****
NI	Number	1979-2014	**0.01**	**0.02**	-0.04
		1990-2014	**-0.07**	**-0.04**	**-0.06**
	Duration	1979-2014	**0.16**	**0.11**	-0.14
		1990-2014	**-0.48**	**-0.14**	**-0.58**
	Intensity	1979-2014	-0.09	0.03	0.03
		1990-2014	**0.27**	**0.03**	**0.01**
	Intensity-C	1979-2014	-0.09	0.01	0.02
		1990-2014	**0.27**	**0.06**	-0.01

Table S6: Correlation coefficients of global TC activity (number, days, intensity) between RGTracks-20C (UZ-based results) and IBTrACS with the ENP and NI included and excluded, respectively. Asterisks indicate the confidence levels,1 asterisk (*) = 90%, 2 asterisks (**) = 95%, and 3 asterisks (***) = 99%.

Characteristics	Region	UZ	RGTracks-20C
Number	ENP & NI included	0.65***	0.68***
	ENP & NI excluded	0.67***	0.87***
Days	ENP & NI included	0.78***	0.63***
	ENP & NI excluded	0.85***	0.70***
Corrected Intensity	ENP & NI included	0.58***	0.84***
	ENP & NI excluded	0.65***	0.85***

Table S7: As in Table S4, but with ENP and NI basins included and excluded, respectively.

Characteristics	Dataset	ENP & NI included	ENP & NI excluded
Number	IBTrACS	**-0.06**	**0.04**
	UZ	**-0.01**	-0.19**
	RGTracks-20C	0.19	**0.08**
Duration	IBTrACS	**-2.70**	**-2.83***
	UZ	**-0.29**	**-1.37***
	RGTracks-20C	1.82	0.10
Intensity	IBTrACS	**0.17*****	**0.12*****
	UZ	**0.03**	**0.02**
	OWZ	**0.05*****	**0.05*****
	UZ-C	**0.04**	**0.02**
	RGTracks-20C-C	**0.09*****	**0.09*****

S5 Case studies

S5.1 1992 'Andrew' hurricane

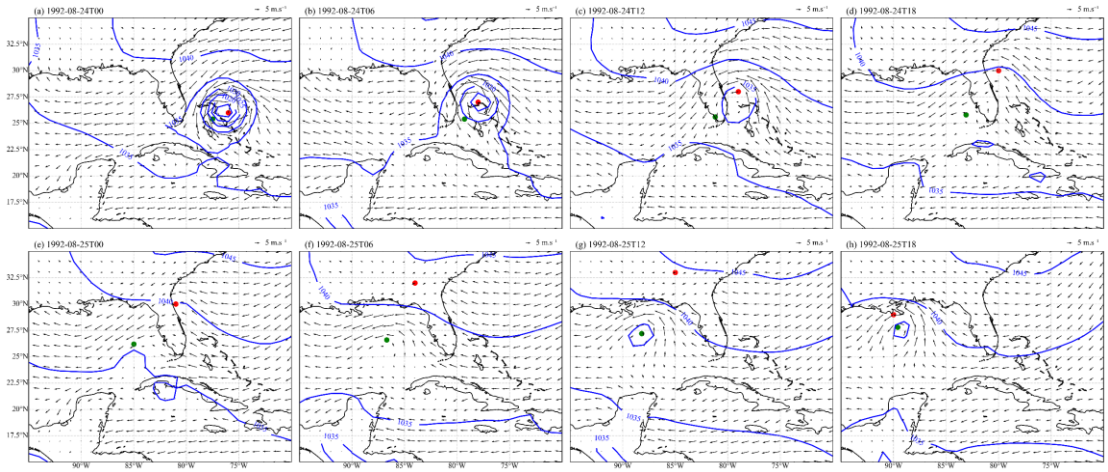

Figure S9: Hurricane Andrew's August 24-25, 1992, sea level pressure (unit: hPa) and wind speed at 10 m (unit: $m \cdot s^{-1}$) obtained from 20CRv3.

S5.2 1928 'Okeechobee' hurricane

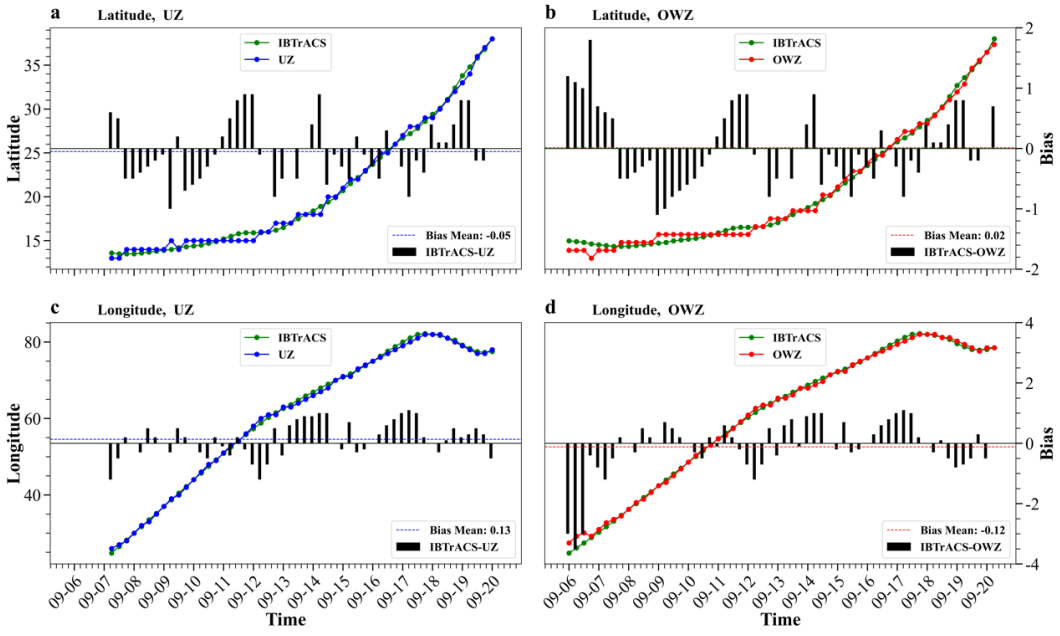

Figure S10: Position records of Hurricane Okeechobee from IBTrACS, RGTracks-20C (The red dotted line represents the identification of TCs from the 20CRv3 reanalysis based on OWZ tracker) and UZ tracker, and analysis of positional bias between these two datasets. a-b, latitude (unit: °) records for Hurricane Okeechobee as reported by IBTrACS and the UZ tracker (a) and RGTracks-20C(b), with corresponding bias values shown in bar and dashed lines represent (UZ: -0.05, RGTracks-20C: 0.02). c-d, longitude (unit: °) records for Hurricane Okeechobee as reported by IBTrACS (green) and the UZ (blue) (c) and RGTracks-20C (red) (d) trackers, with corresponding bias values shown in bar and dashed lines represent (UZ: 0.13, RGTracks-20C: -0.12).

Table S8: Intensities (SLP_{min}) of Hurricane Okeechobee recorded in IBTrACS, RGTracks-20C and UZ tracker. The World Meteorological Organization (WMO) and the United States of America (USA) agencies in IBTrACS recorded the hurricane intensities. UZ and RGTracks-20C indicate the SLP_{min} directly obtained from 20CRv3, while UZ-C and RGTracks-20C -C represent bias-corrected results based on observational data.

Time	WMO	USA	UZ	RGTracks -20C	UZ-C	RGTracks -20C-C
1928/9/12 18:00	940	940	971	972	955	940
1928/9/13 18:00	931	931	958	958	930	920
1928/9/13 21:00		936				
1928/9/14 0:00	941	94	958.	958	930	920
1928/9/17 0:00	929	929	955	955	925	915
1928/9/18 6:00	977	977	958	958	982	965
1928/9/18 9:00		976				
1928/9/18 12:00	976	976	985	985	982	965
1928/9/18 15:00		976				
1928/9/18 18:00	977	977	986	986	983	966
1928/9/18 19:00	977	977				
1928/9/20 12:00	1008	1008				
1928/9/20 15:00		1006				
1928/9/20 18:00		1005				

S5.3 1920 '1920232N24150' Typhoon in the WNP

The typhoon labeled '1920232N24150' occurred in the WNP in 1920. According to meteorological records from Kagawa Prefecture of Japan (https://www.shikoku-saigai.com/archives/25443?preurl&query_pref&query_city&query_dis_kind&query_s=%E5%8F%B0%E9%A2%A8+&query_date=18680908-19261225&query_paged=11), the typhoon brought 20 to 110 mm of rainfall to the region between August 20 and 21. Although the typhoon had a short duration and caused relatively low rainfall, it damaged crops, particularly fruit trees and vegetables, indicating that it made landfall in Japan.

While the IBTrACS provides a record of this typhoon, it includes only part of the storm's tracks, especially missing the tracks during its landfall in Japan (August 20–21). However, the RGTracks-20C

successfully reconstructs the typhoon's tracks. To verify the accuracy of the track in the RGTracks-20C, we used the 20CRv3 to generate sea level pressure maps for August 19 to 21, 1920, and compared them with historical weather chart archives (Figs. S11–13).

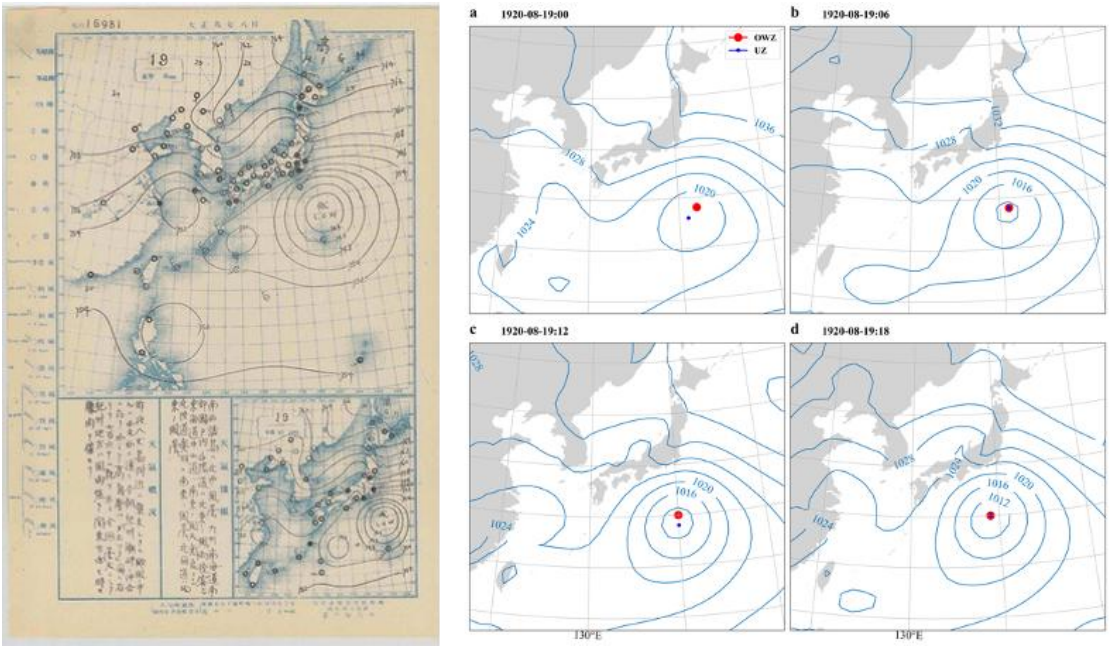

Figure S11: Comparison of the historical Asia-Pacific weather map and sea-level pressure from 20CRv3 for the 1920 typhoon '1920232N24150' on August 19, 1920. On the left is a historical Asia-Pacific weather map provided by the National Institute of Informatics (NII). a-d, Sea level pressure on August 20, 1920 at 00:00 (a), 06:00 (b), 12:00 (c), and 18:00 (d) based on 20CRv3. The blue and red dots indicate the positions of the typhoon as identified by the UZ (blue) and OWZ (red) trackers, respectively. The historical weather chart was created by NII "Digital Typhoon" based on "Weather Charts" from Japan Meteorological Agency and obtained from https://agora.ex.nii.ac.jp/digital-typhoon/weather-chart/.

Historical weather charts provided by the National Institute of Informatics (NII) confirm the presence of a low-pressure system southeast of Japan on August 19 (Fig. S11). By August 20 (Fig. S12), the system was moving northwestward, approaching the Japanese coast, and by August 21 (Fig. S13), it was located over Japan's southern islands, further confirming its landfall.

A comparison with historical weather charts shows that the low-pressure system in 20CRv3 closely matches the observation records, indicating that 20CRv3 effectively simulated the typhoon's development and landfall in Japan. Thus, RGTracks-20C not only captures the typhoon's tracks but also accurately represents the pre-landfall (Fig. S11), landfall (Fig. S12), and post-landfall phases (Fig. S13). This reconstruction fills the gaps in IBTrACS regarding the missing tracks of the typhoon during this period.

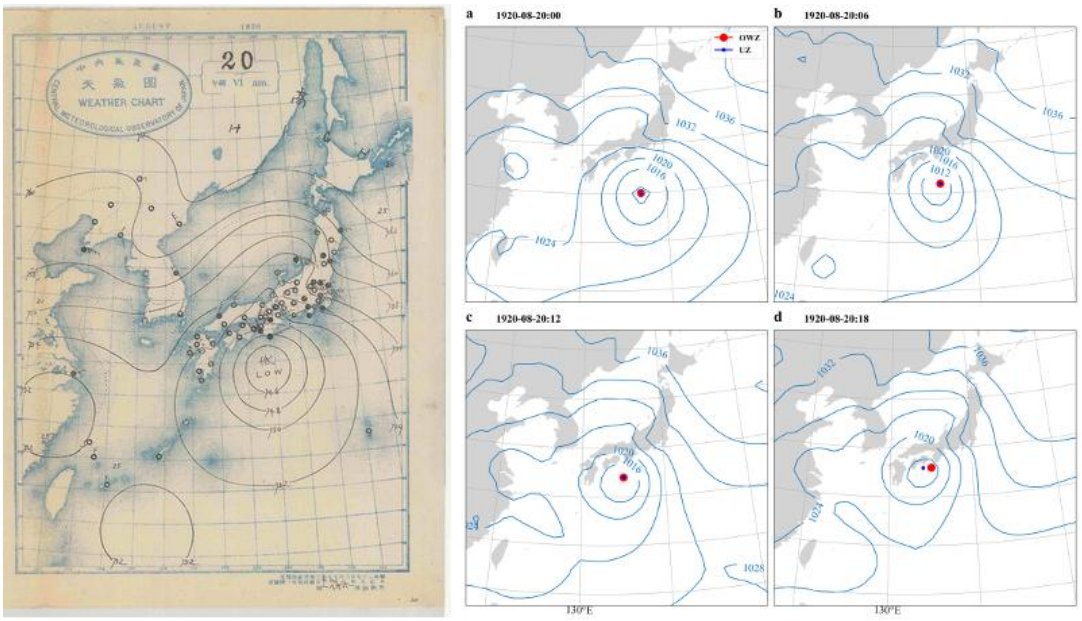

Figure S12: As shown in Fig. S11, but for August 20, 1920. The historical weather chart was created by NII "Digital Typhoon" based on "Weather Charts" from Japan Meteorological Agency and obtained from https://agora.ex.nii.ac.jp/digital-typhoon/weather-chart/.

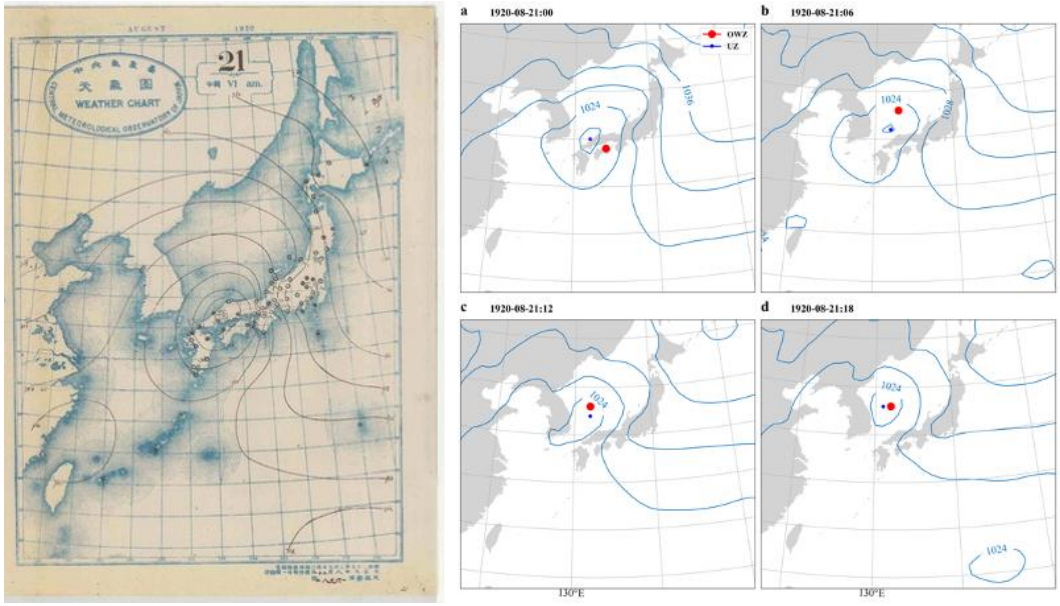

Figure S13: As shown in Fig. S11, but for August 21, 1920. The historical weather chart was created by NII "Digital Typhoon" based on "Weather Charts" from Japan Meteorological Agency and obtained from https://agora.ex.nii.ac.jp/digital-typhoon/weather-chart/.

S6 Impacts of assimilating IBTrACS in the 20CRv3

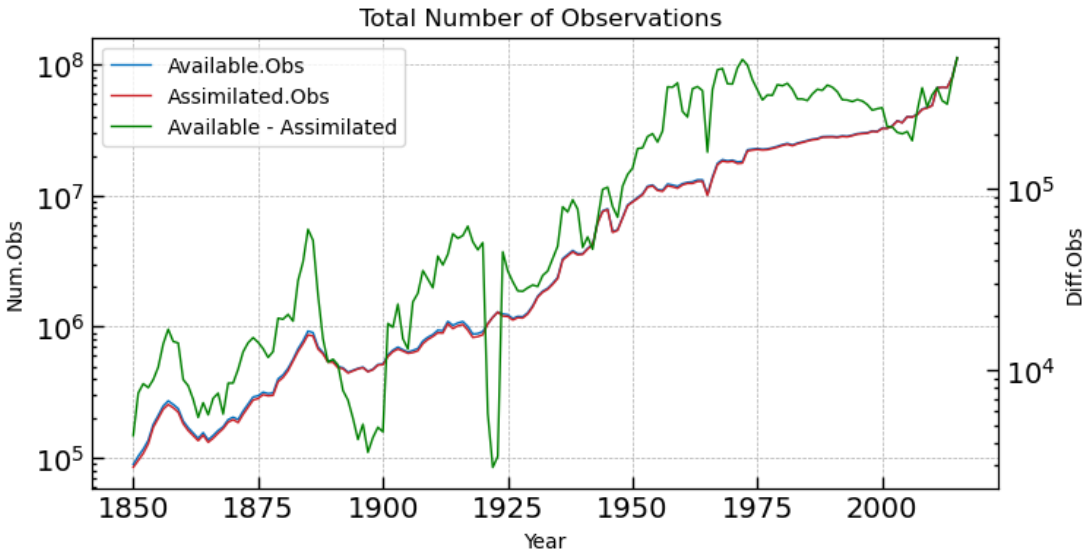

Figure S14: Time series of the total number of available and assimilable observations from 1850 to 2015. Blue and red lines represent assimilable and assimilated observations, respectively. And the green line indicates the difference between the available and assimilated observations.

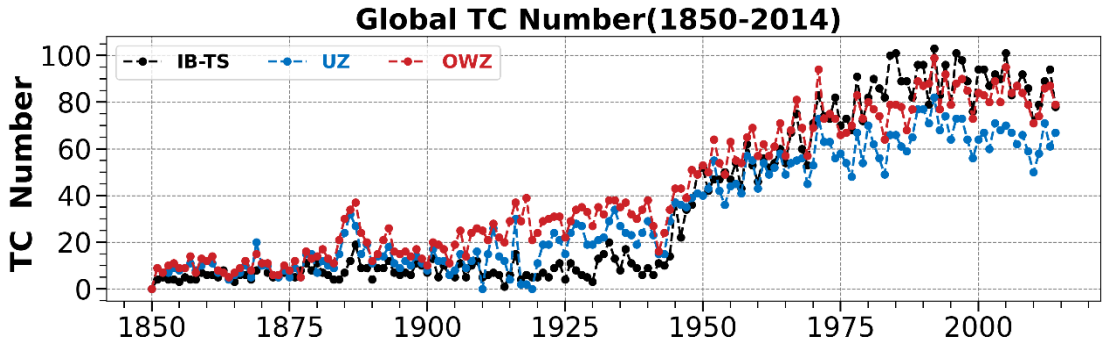

Figure S15: Time series of the TC number from 1850 to 2014. The black dotted line represents the IBTrACS, while the blue and red dotted lines represent UZ tracker and RGTracks-20C, respectively.

References

Accarino, G., Donno, D., Immorlano, F., Elia, D., and Aloisio, G.: An Ensemble Machine Learning Approach for Tropical Cyclone Localization and Tracking From ERA5 Reanalysis Data, Earth Space Sci., 10, e2023EA003106, https://doi.org/10.1029/2023EA003106, 2023.

Bell, S. S., Chand, S. S., Tory, K. J., and Turville, C.: Statistical Assessment of the OWZ Tropical Cyclone Tracking Scheme in ERA-Interim, J. Clim., 31, 2217–2232, https://doi.org/10.1175/JCLI-D-17-0548.1, 2018.

Bourdin, S., Fromang, S., Dulac, W., Cattiaux, J., and Chauvin, F.: Intercomparison of four algorithms for detecting tropical cyclones using ERA5, Geosci. Model Dev., 15, 6759–6786, https://doi.org/10.5194/gmd-15-6759-2022, 2022.